Biochemical and Biophysical Research Communications 459 (2015) 521–528

Contents lists available at ScienceDirect

Biochemical and Biophysical Research Communications

journal homepage: www.elsevier.com/locate/ybbrc

Nanoscale analysis of unstained biological specimens in water without radiation damage using high-resolution frequency transmission electric-field system based on FE-SEM

Toshihiko Ogura

Biomedical Research Institute, National Institute of Advanced Industrial Science and Technology (AIST), Central 2, Umezono, Tsukuba, Ibaraki 305-8568, Japan

ARTICLE INFO

Article history:
Received 20 February 2015
Available online 5 March 2015

Keywords:
Scanning electron microscopy
Frequency transmission electric-field
Wet biological specimens
Unstained protein particle
Nanoscale analysis

ABSTRACT

Scanning electron microscopy (SEM) has been widely used to examine biological specimens of bacteria, viruses and proteins. Until now, atmospheric and/or wet biological specimens have been examined using various atmospheric holders or special equipment involving SEM. Unfortunately, they undergo heavy radiation damage by the direct electron beam. In addition, images of unstained biological samples in water yield poor contrast. We recently developed a new analytical technology involving a frequency transmission electric-field (FTE) method based on thermionic SEM. This method is suitable for high-contrast imaging of unstained biological specimens. Our aim was to optimise the method. Here we describe a high-resolution FTE system based on field-emission SEM; it allows for imaging and nanoscale examination of various biological specimens in water without radiation damage. The spatial resolution is 8 nm, which is higher than 41 nm of the existing FTE system. Our new method can be easily utilised for examination of unstained biological specimens including bacteria, viruses and protein complexes. Furthermore, our high-resolution FTE system can be used for diverse liquid samples across a broad range of scientific fields, e.g. nanoparticles, nanotubes and organic and catalytic materials.

1. Introduction

Electron microscopy is an important tool for high-resolution imaging of not only materials but also various biological specimens; in particular, it allows for examination of bacteria and protein structures [1–4]. Moreover, scanning electron microscopy (SEM) has been widely used to analyse bacterial and viral surface structures [5–9]. However, to avoid electrical radiation damage and vacuum damage [10,11], SEM of biological specimens requires special sample preparation protocols involving glutaraldehyde fixation, negative staining, cryo-techniques and/or metal coating [5,8,9,12]. These protocols also enhance a specimen's contrast and prevent artefacts caused by the electrical charge. Until now, atmospheric and/or wet biological specimens have been examined by means of various atmospheric holders [13,14] or special equipment [15,16], but they undergo heavy radiation damage by the direct electron beam (EB) [10,11]. In addition, images of unstained biological samples in water yield poor contrast because specimens consisting of lightweight materials and water scatter the electron beam. Therefore, these systems require additional glutaraldehyde fixation with negative staining or metal labelling [13,14].

We recently developed a new imaging technology called the frequency transmission electric-field (FTE) system, which is based on thermionic SEM; the latter allows for examination of unstained biological specimens in water [17,18]. Our FTE method produces high-contrast images of unstained and unfixed biological specimens introduced in a liquid sample holder comprising two silicon nitride (SiN) films [17]. In this method, the biological samples are not exposed directly to the EB; this approach prevents electron radiation damage [17]. Moreover, we developed a high-sensitivity FTE system, which allows for 100-fold enhancement of the signal by −30 V bias voltage applied to the tungsten-coated SiN film [18]. This enhancement is expected to considerably reduce the EB current, thereby improving spatial resolution and the signal-to-noise (S/N) ratio. Nonetheless, the existing FTE system was developed using thermionic emission SEM. Therefore, resolution is limited to approximately 10,000× magnification [17,18].

In this study, we present a high-resolution FTE system based on field-emission (FE) SEM. This system is suitable for high-resolution

E-mail address: t-ogura@aist.go.jp.

http://dx.doi.org/10.1016/j.bbrc.2015.02.140

examination of intact bacteria, viruses and protein particles in water without radiation damage.

2. Materials and methods

2.1. Metal deposition on the upper SiN film

A 50-nm-thick SiN film supported by a 0.4 × 0.4 mm window in a Si frame (4 × 4 mm, 0.38 mm thick, Silson Ltd., UK) was coated with tungsten using a magnetron sputtering device (Model MSP-30T, Vacuum Device Inc., Japan). Tungsten was spattered for 15 s at 0.8 Pa argon pressure and 200 mA, producing a 15-nm-thick coating. The distance between the sputter target and the SiN film was 50 mm.

2.2. Sample preparation

The purple, rod-shaped, non-sulphur photosynthetic bacterium *Rhodobacter capsulatus* [19–21] was obtained from the Santechno Co. (Japan, Osaka). The bacterial suspension (1 ml) was centrifuged at 6200 rpm for 1 min in Capsulefuge PMC-060 (Tomy Inc., Japan) and the supernatant was replaced by 0.5 ml of an aqueous solution of 1% (w/v) trehalose (Hayashibara Inc., Japan) and 0.5% NaCl. The sample solution (2 μl) was placed in a liquid-sample holder.

The *Spodoptera litura* nuclear polyhedrosis virus (SNPV) was provided by Nippon Kayaku Co. Ltd. (Japan). The SNPV powder (10 mg) was resuspended in a 20 mM sodium carbonate solution (pH 11.0, 1 ml) for 10 min, and the resulting baculovirus suspension (2 μl) was placed in the holder.

A mouse IgM antibody solution (catalogue number M079-3) was obtained from Medical & Biological Laboratories Co., Ltd. (Japan). A 7-μl aliquot of the IgM solution was diluted to 14 μl with distilled water. A 3 μl aliquot of the diluted solution was placed in the liquid-sample holder.

2.3. The liquid-sample holder and stage

Our sample holder consisting of an upper aluminium (Al) part and a lower acrylic resin part maintained the sample solution at atmospheric pressure between the SiN films (Fig. 1A). The upper tungsten (W)-coated SiN film was attached to the Al part by a two-sided sticky tape (No. 7602, Teraoka Seisakusho Co., Ltd, Japan). The tungsten layer was connected to the Al holder using silver conductive ink (CW2900, ITW Chemtronics, USA). To seal the two SiN films containing the liquid sample, the holder parts were locked by an O-ring and four screws (Fig. 1B). The Al holder part received voltage bias from three nickel–hydrogen batteries (9 V each), with the total bias voltage of approximately −27 V. The resin holder part had high electrical resistivity, insulating the terminal underside of the holder from the metal-coated SiN film (Fig. 1B).

2.4. The high-resolution FTE system and FE-SEM setup

The high-resolution FTE imaging system based on FE-SEM is shown in Fig. 1C. A beam-blanking unit (Sanyu Electron Co., Japan) consisting of deflection plates was placed into the FE-SEM device JSM-7000F (JEOL, Japan). The beam-blanking unit was controlled by a function generator (WF1974, NF Co., Japan) using a square wave at the frequency of 30 kHz and voltage 0–3 V; its amplitude was enhanced by an optocoupler module at 0–27 V (HCNW3120, Avago Technologies Limited, USA). The liquid-sample holder was mounted onto the SEM stage, and the detector terminal was connected to a direct current (DC) pre-amplifier (1000× gain) under the holder (Fig. 1B). The electrical frequency signal from the pre-amplifier was fed into the lock-in amplifier (LI5640, NF Co., Japan) after a low-pass–filtered (LPF) (cut-off frequency 100 kHz; Fig. 1C). The LPF signal, lock-in amplifier output and the XY scan signal were logged by a data recorder (EZ7510, NF Co., Japan) at the sampling frequency of 20 kHz. SEM images (1280 × 960 pixels) were captured at magnification 2000–50,000×, scanning time 120 s, working distance 7 mm, EB acceleration voltage 3.6–4 kV and current 200–600 pA.

2.5. Image processing

The FTE signal data from the data recorder were transferred to a personal computer (Intel Core i7, 2.8 GHz, Windows 7), and high-resolution FTE images of the LPF signal and lock-in-amplifier signal (30 kHz) were processed using the Matlab R2007b software with an image processing toolbox (Math Works Inc., USA). Original FTE images were filtered using a two-dimensional (2D) Gaussian filter (GF) with the kernel size of 7 × 7 pixels and the radius of 1.2σ. Background subtraction was achieved by subtracting FTE images from the filtered images using a broad GF (91 × 91 pixels, 50σ).

3. Results

A schematic of the high-resolution FTE system based on FE-SEM is shown in Fig. 1. A liquid-sample holder consists of an Al part and acrylic lysine part (Fig. 1A). A 50-nm-thick SiN film supported by a silicon frame was attached to the Al holder part using a two-sided sticky tape (Fig. 1B, left). The SiN film was coated by a 15-nm-thick tungsten layer. Another SiN film was embedded in an acrylic resin part (Fig. 1A, right). Intact biological specimens in water were introduced into the space between the two SiN films. Both holder parts were sealed by an O-ring using four screws (Fig. 1B), maintaining the sample environment at near-atmospheric pressure. The liquid-sample holder for biological specimens was attached to the circuit breadboard of a direct current (DC) pre-amplifier mounted onto a sample stage (Fig. 1B). This ensemble was introduced into a FE-SEM chamber via a sample transfer chamber. In the FE-SEM chamber, the sample holder on the DC pre-amplifier stage was connected to an outside bias source and to a signal detection system through a connector (Fig. 1C).

The beam-blanking unit installed in the FE-SEM instrument served as an electrostatic deflection system. A 30 kHz square wave was used as a control signal and was applied to the deflection plate to produce a focused-modulation EB (Fig. 1C). The tungsten-coated SiN film was irradiated using the resulting chopped EB at low-acceleration voltage of 3.6–4.0 kV. Its low-acceleration electrons were almost absorbed by the tungsten layer (Supplementary Fig. 1); thus, the negative electric-field potential arose at this site. Moreover, radiation damage to the biological specimens was prevented by the tungsten-coated SiN film. A detector terminal under the sample holder received the electrical signal passing through the EB-irradiated area in the biological specimen [17]. This signal was amplified by a DC pre-amplifier before a low-pass filter, and then was directly recorded by a data recorder as a LPF signal (Fig. 1C). The 30 kHz signal was obtained using a lock-in amplifier. Finally, the output and EB scan signals from the data recorder generated FTE images from the LPF signal and the 30 kHz lock-in amplifier output.

With this high-resolution FTE system, we first examined unstained and unfixed bacteria *Rhodobacter capsulatus* [19–21] in water. Fig. 1D and E shows the LPF signal and the 30 kHz signal images of intact bacteria under 3.6 kV EB acceleration, 2000× magnification and −27 V bias voltage. In both images, the unstained bacteria appeared black (with contrast) and had an elongated shape, which were 2–5 μm long and 0.5–1.0 μm wide. In this case, the S/N ratio of the LPF image was slightly better than that of

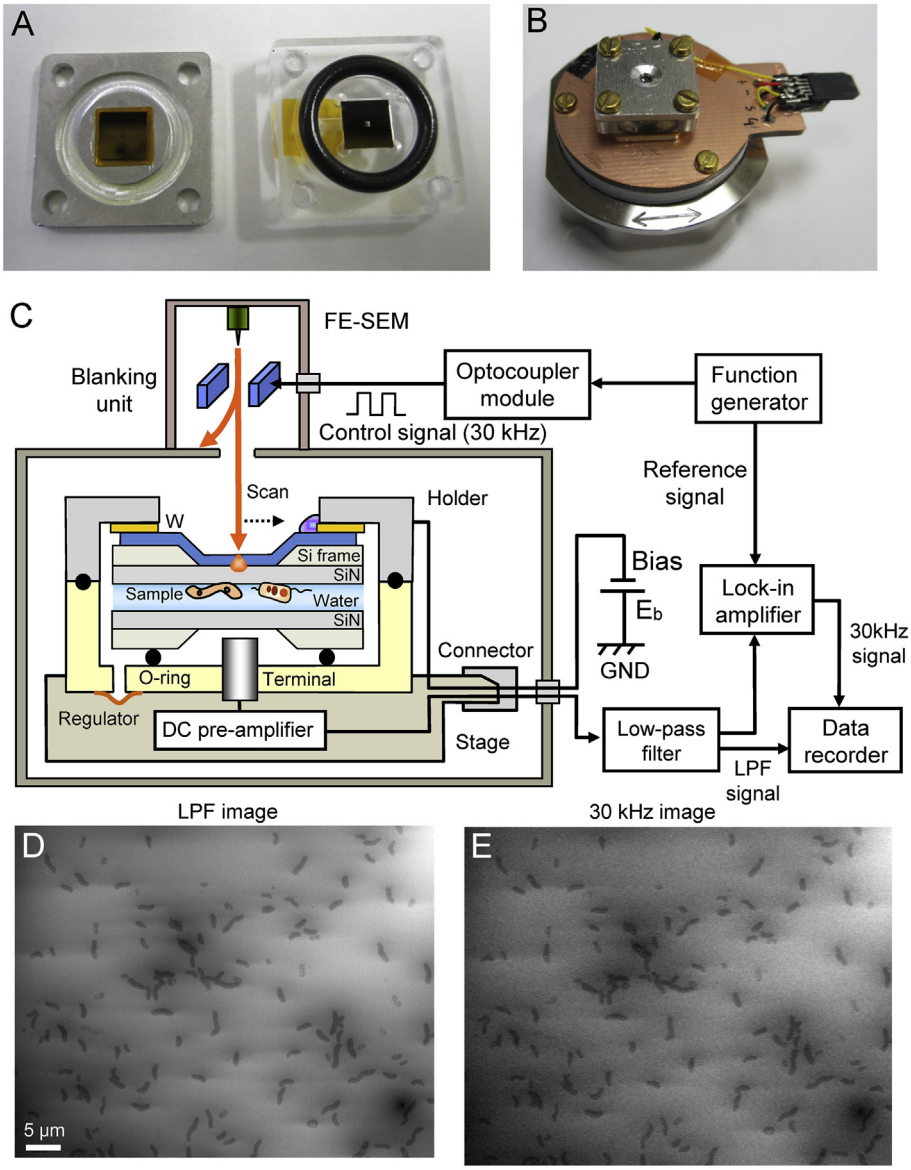

Fig. 1. Experimental set-up and the high-resolution frequency transmission electric-field (FTE) system. (A) A photograph of parts of the liquid-sample holder; the left side is an Al part with a W-coated SiN film. The right side is an acrylic lysine part in 50 nm SiN film. The holder width is 15 mm. (B) The liquid-sample holder parts are sealed by an O-ring using four screws. The sample holder with biological specimens is mounted on the DC pre-amplifier attached to the sample stage. (C) A schematic of the electrical high-resolution FTE system based on FE-SEM. Biological specimens in water were injected into the space between two SiN films in the sample holder. The scanning EB is modulated by a beam-blanking unit using a 30 kHz square wave from a function generator, which is applied to the W-coated SiN film at 3.6- to 4.0-kV acceleration voltage. The measurement terminal under the holder detects the electrical frequency signal from the W layer. Its signal is amplified by a DC pre-amplifier under the sample holder; this signal goes outside the microscope via a connecter. An LPF signal and lock-in amplifier output (30 kHz signal) are recorded by a data recorder. The bias voltage is applied to the tungsten layer via the connector. (D) An LPF signal image of unstained bacteria *Rhodobacter capsulatus* in water according to the high-resolution FTE system; the image was obtained with a 3.6 kV EB, 2000× magnification and −27 V bias voltage. The scale bar is 5 μm. (E) The 30 kHz image from lock-in amplifier output. The 30 kHz image and its LPF version are obtained simultaneously.

the 30 kHz signal image. Furthermore, the background of both FTE images was slightly undulated; this phenomenon reflects the difference in water thickness between the two SiN films. If water thickness fluctuated strongly, the background contrast was strongly undulated (Supplementary Fig. 2A–C). Therefore, to determine the sample structure, the undulated background was subtracted from the broad GF image (Supplementary Fig. 2D and E). Moreover, the reversed-contrast image of bacteria showed clear-cut structure (Supplementary Fig. 2F).

The unstained bacteria in water were further analysed at high magnification (Supplementary Fig. 3). The intact bacteria immersed in water were examined using the high-resolution FTE system at 5000× magnification, 3.6 kV EB acceleration and −27 V bias. To visualise the bacteria clearly, the background in the original LPF image was subtracted after application of reversed contrast (Fig. 2A). The bacteria were visible with clear-cut white contrast; the inner structure exhibited complex undulation. The bacteria indicated by white arrows in Fig. 2A were magnified for detailed analysis (Fig. 2B and C). A thin fibre was clearly detectable within the bacterial cell (Fig. 2B, the white arrow) and was attributed to flagella (12- to 25-nm diameter) [22]. Furthermore, the bacteria were connected to each other by small knobs (Fig. 2B and C, red arrows). This connection probably means an initial stage of biofilm formation [9,23]. The pseudo-colour map and a 3D colour map of bacteria indicated by the lower white arrow in Fig. 2A shows clear-cut inner structure (Fig. 2D and E). These colour maps clearly

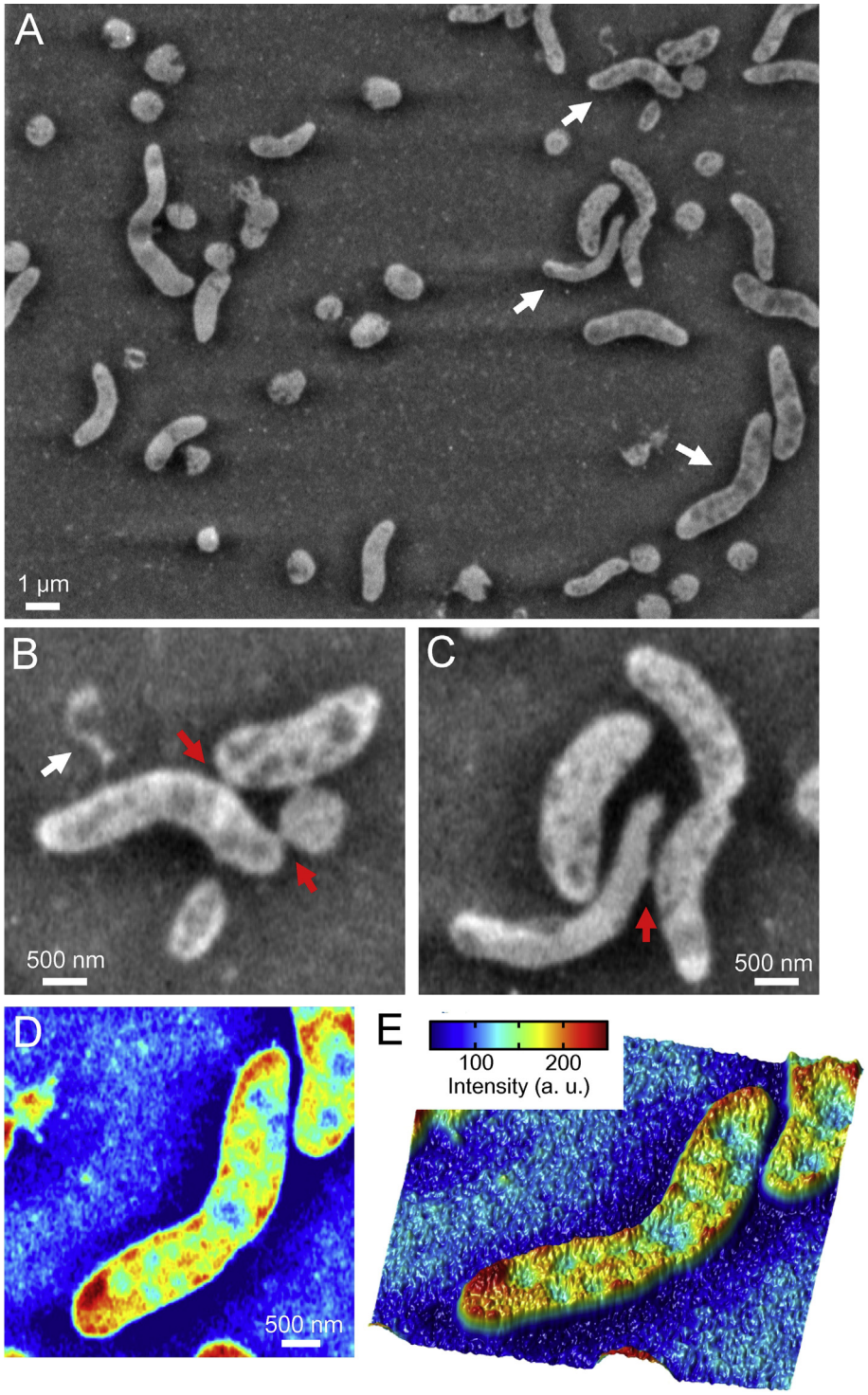

Fig. 2. Imaging of intact bacteria in water by means of the high-resolution FTE system. (A) A reversed-contrast image of *Rhodobacter capsulatus* from an LPF signal; the image was filtered using a 2D Gaussian filter (GF; 7 × 7 pixels, σ = 1.2) after background subtraction of a filtered image: the broad 2D GF (91 × 91 pixels, σ = 50) image. The image was obtained with a 3.6 kV EB, 5000× magnification and −27 V bias. The bacteria show clear-cut white contrast; the inner structure exhibits complex undulation. (B) A magnified image of the top right bacteria indicated with a white arrow in (A). The white arrow indicates flagella. (C) A magnified image of the middle right bacteria in (A). The red arrows indicate the bacterial connection. (D) A magnified pseudo-colour image of the bottom right bacterium in (A). (E) A 3D colour map of the same bacterium. The colour map and 3D map clearly show inner structure: a small grain and a high-density region. The scale bar is 1 μm in (A) and 500 nm in (B)–(D). (For interpretation of the references to colour in this figure legend, the reader is referred to the web version of this article.)

showed a high-density region at one end of a bacterium; this finding is suggestive of the presence of a nucleoid [24,25]. The centre of the bacterium contained many small circles and large ellipsoid low-density regions (Fig. 2D and E); these structural images are in accord with thin-slice images of bacteria obtained by means of transmission electron microscopy (TEM) [19,24–26].

Next, we examined an unstained baculovirus in water by means of the high-resolution FTE system; the virus appeared rod-shaped,

200–350 nm long, with a diameter ranging between 60 and 100 nm [27–29]. The virions in water appeared as small rod-shaped particles with clear white contrast at 40,000× magnification, a 3.6 kV EB and −27 V bias voltage (Fig. 3A). Three magnified baculovirus images (Fig. 3B–D) and the pseudo-colour map (Fig. 3E–G) clearly showed rod-shaped structure. Furthermore, the virion contained a small grain at one end (Fig. 3C and F) consisting of the envelope [27].

Finally, we also used the new method to analyse unstained and unfixed IgM antibody molecules in water. The IgM antibody has

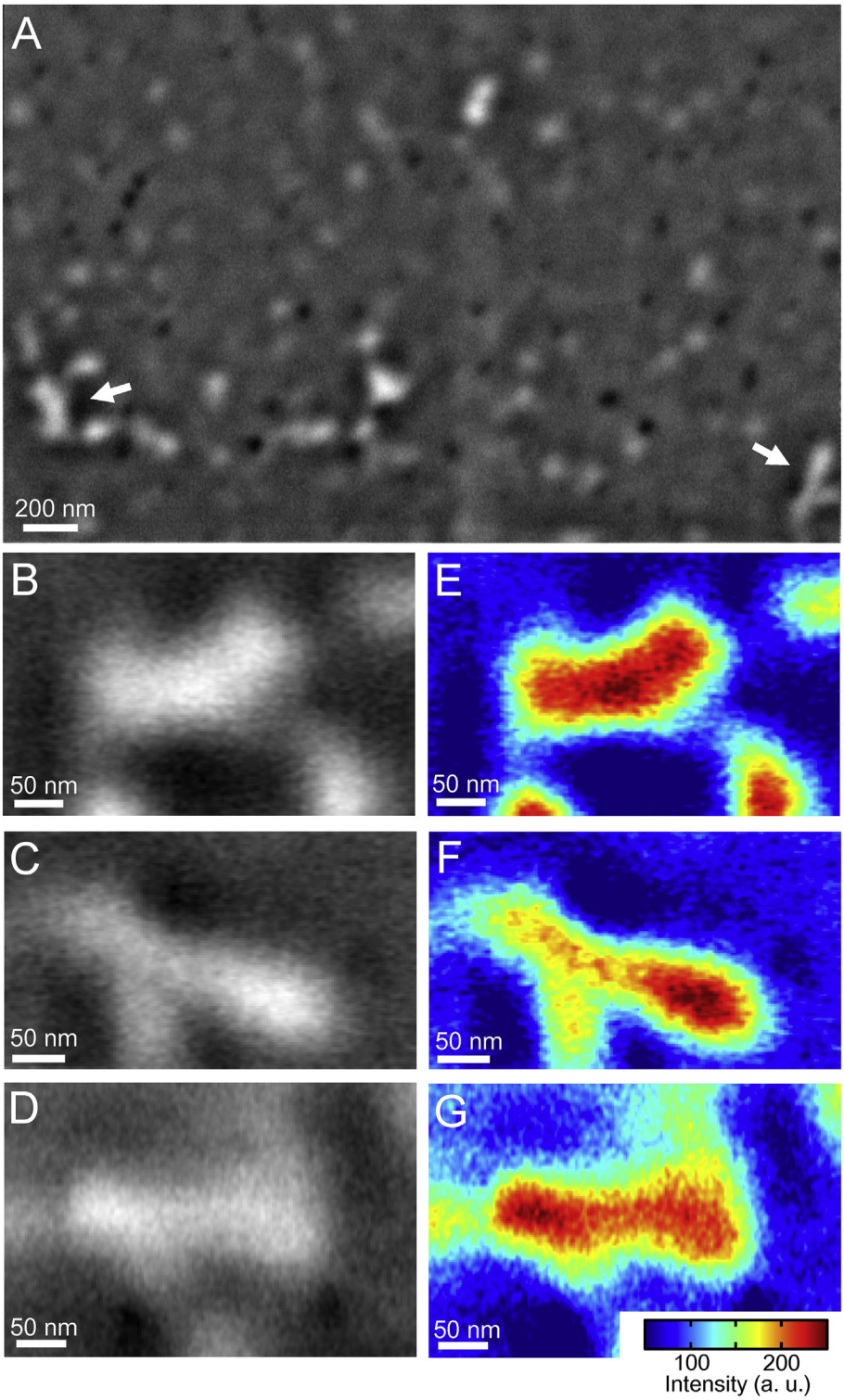

Fig. 3. Imaging of an intact baculovirus in water by means of the high-resolution FTE system. (A) An image of an unstained and unfixed baculovirus in water, obtained using the LPF signal. This picture was taken at 40,000× magnification, 3.6 kV EB acceleration voltage and −27 V bias. (B and C) Magnified images of the baculovirus shown on the left and right side. (D) A magnified image from another scanned image. (E–G) Pseudo-colour maps of (B–D). The scale bar is 200 nm in (A) and 50 nm in (B)–(G). (For interpretation of the references to colour in this figure legend, the reader is referred to the web version of this article.)

molecular weight of 900 kDa and consists of five IgG antibodies [30–32]. The IgM pentamer is star-shaped, with a diameter of approximately 45 nm; its centre is highly dense with a dome-like shape [32]. We examined intact IgM protein in water at 50,000× magnification and 4 kV EB acceleration of a 30 kHz signal (Fig. 4A). Several small particles of approximately 50 nm diameter were dispersed throughout the whole visual field. Fig. 4B shows three individual IgM molecules indicated in Fig. 4A with white arrows, and the pseudo-colour maps are shown in Fig. 4C. Individual IgM molecules are visible as slightly star shaped with a dome-like centre. These results are consistent with a previously reported negatively stained TEM and cryo-atomic force microscopy (AFM) images [30–32]. In 3D colour maps (Fig. 4D), the star-like shape was visible more clearly. However, the IgG-like arms exhibited blurry structure. The line plot across the IgM centre (Fig. 4B, centre, dashed line) is shown in Fig. 4E and F. The spatial resolution of the high-resolution FTE method based on FE-SEM is 8 nm with the normalised intensity width that decreases from 0.75 to 0.25 (Fig. 4F); this resolution is much better than 41 nm of the existing thermionic SEM system [17,18].

4. Discussion

During general SEM examination, the contrast of biological specimens in water with the liquid sample holder is very low because of a weak interaction of the EB with lightweight atoms in

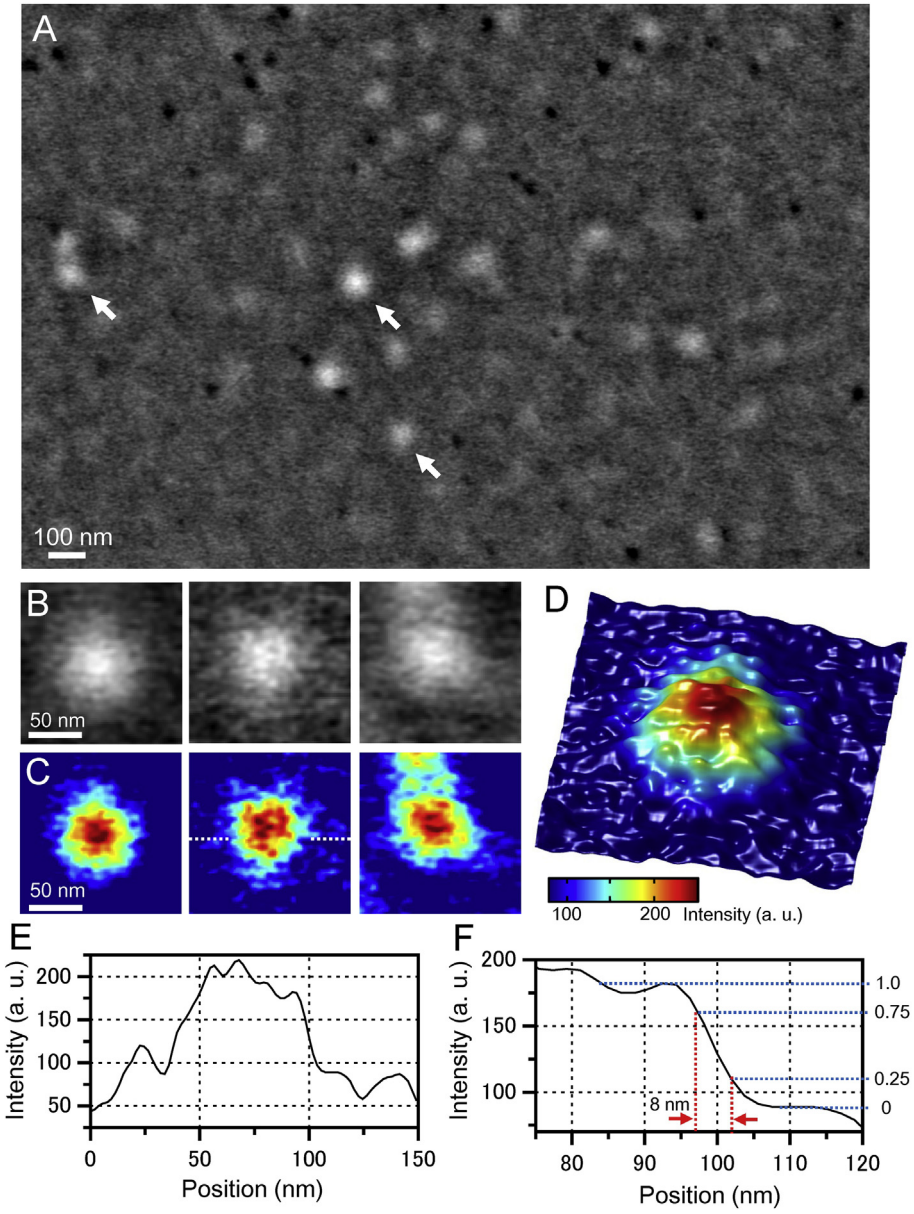

Fig. 4. Examination of an intact IgM antibody in water. (A) The 30 kHz signal image of unstained mouse IgM particles in water obtained using our high-resolution FTE system. The image scan conditions were as follows: magnification 50,000×, 3.6 kV EB acceleration and −27 V bias voltage. Many particles of approximately 50 nm diameter are dispersed throughout the whole visual field. (B) Three individual IgM molecules indicated with white arrows in (A). (C) Pseudo-colour maps of (B). Individual IgM molecules are visible as slightly star-shaped with a dome-like centre. (D) A 3D colour map of the IgM molecules on the left side of (C). The star-like shape is more clear-cut. (E) A line plot across the IgM particle centre indicated in (C) with a dashed line. A.u. = arbitrary units. (F) A line plot of the right-side edge in the IgM molecule. Spatial resolution of the high-resolution FTE system is 8 nm. This measure is defined as the width over which the normalised intensity decreases from 0.75 to 0.25 in the line plot. The scale bar is 100 nm in (A) and 50 nm in (B) and (C). (For interpretation of the references to colour in this figure legend, the reader is referred to the web version of this article.)

the sample. Furthermore, the EB is scattered and absorbed not only by the sample but also by water. Therefore, the high-resolution and high-contrast imaging of intact biological specimens immersed in water is problematic. Moreover, the biological specimens undergo heavy radiation damage by the EB [10,11]. In contrast, our new FTE system with the bias voltage technology enables examination of unstained biological samples in water [17,18]. The electrons are absorbed by the tungsten-coated SiN film covering the specimens; hence, our method is suitable for low radiation damage examination.

In this study, we developed a high-resolution FTE system that is introduced into a FE-SEM chamber (Fig. 1A–C). Our new FTE system allows for simultaneous examination of an LPF signal image and a lock-in amplifier image (Fig. 1D and E). Our system clearly reveals the inner structure of intact bacteria in water (Fig. 2). The bacterium images show a high-density region and a spherical low-density particle (Fig. 2). Its structure is suggestive of a nucleoid with a spherical intracytoplasmic membrane [24,25]. Analysis of the spherical intracytoplasmic membrane generally involves preparation of thin sections of a bacterium after negative staining and/or fixation [19,26]. In contrast, our method allows for high-resolution examination of intact and untreated bacteria in water. Furthermore, we examined an unstained and unfixed baculovirus and IgM protein particles at 40,000–50,000× magnification (Figs. 3 and 4). These results suggest that the new FE-SEM-based FTE system has resolution that is higher than the existing thermionic-SEM-based FTE system [18]. Moreover, our FTE imaging yields transmission images depending on the sample volume. Therefore, a 3D volume structure can probably be obtained by means of many tilted sample images using the sensor array detector [33].

The spatial resolution of our new FTE method is 8 nm, which is enough to analyse bacteria and viruses in water (Figs. 2 and 3). Nonetheless, at present, our method is not suitable for detailed structural analysis of the IgG arms of an IgM antibody (Fig. 4). In structural analysis of a protein particle, the desired resolution is better than 5 nm. In our system, the specimens are attached under the tungsten-coated SiN film, with the total thickness 65 nm (tungsten layer: 15 nm, SiN film: 50 nm), which is wider than the IgM diameter (45 nm).

Spatial resolution of an FTE image is influenced by the thickness of the tungsten-coated SiN film. Therefore, we are planning on improving the spatial resolution in the sample holder using a SiN film thinner than 50 nm. The SiN film thickness has recently been reduced to 10 nm by some biotech companies; this thinner film is probably effective at improving the 5 nm spatial resolution. We expect our next high-resolution FTE system to offer spatial resolution better than 5 nm, with 3D structural analysis using a linear array detection system [33].

In conclusion, we developed a high-resolution FTE system based on FE-SEM. This system allows for high-resolution imaging of unstained bacteria, viruses and protein particles in water without radiation damage. The bacterium images show clear-cut inner structure and flagella. Furthermore, the images of a virus and IgM protein particles reveal cylindrical structure and a star-like shape, respectively; the spatial resolution is 8 nm. Our new method can be easily utilised for analysis of various unfixed and unstained biological specimens including proteins, protein complexes and viruses in water. Furthermore, our FTE method can be applied to diverse liquid samples across a broad range of scientific fields, for example, nanoparticles, nanotubes and organic and catalytic materials.

Conflict of interest

The authors declare no conflict of interest.

Acknowledgments

This study was supported by a KAKENHI Grant-in-Aid for Scientific Research (B) and for the Exploratory Research from the Japan Society for Promotion of Science.

Appendix A. Supplementary data

Supplementary data related to this article can be found at http://dx.doi.org/10.1016/j.bbrc.2015.02.140.

Transparency document

Transparency document related to this article can be found online at http://dx.doi.org/10.1016/j.bbrc.2015.02.140.

References

[1] A. Sali, R. Glaeser, T. Earnest, et al., From words to literature in structural proteomics, Nature 422 (2003) 216–225.
[2] V. Lucic, A. Rigort, W. Baumeister, Cryo-electron tomography: the challenge of doing structural biology in situ, J. Cell. Biol. 202 (2013) 407–419.
[3] A. Leis, B. Rockel, L. Andrees, et al., Visualizing cells at the nanoscale, Trends Biochem. Sci. 34 (2009) 60–70.
[4] Y. Inayoshi, H. Minoda, Y. Arai, et al., Direct observation of biological molecules in liquid by environmental phase-plate transmission electron microscopy, Micron 43 (2012) 1091–1098.
[5] E.J. Wood, R.J. Seviour, A.B.M. Siddique, et al., Spherical body formation in the spirochaete *Brachyspira hyodysenteriae*, FEMS Microbiol. Lett. 259 (2006) 14–19.
[6] N. Minoura, S.I. Aiba, M. Higuchi, et al., Attachment and growth of fibroblast cells on silk fibroin, Biochem. Biophys. Res. Commun. 208 (1995) 511–516.
[7] P.M. Motta, S. Makabe, T. Naguro, et al., Oocyte follicle cells association during development of human ovarian follicle. A study by high resolution scanning and transmission electron microscopy, Arch. Histol. Cytol. 57 (1994) 369–394.
[8] R. Lamed, J. Naimark, E. Morgenstern, et al., Scanning electron microscopic delineation of bacterial surface topology using cationized ferritin, J. Microbiol. Meth. 7 (1987) 233–240.
[9] S.R. Richards, R.J. Turner, A comparative study of techniques for the examination of biofilms by scanning electron microscopy, Water Res. 18 (1984) 767–773.
[10] R.F. Egerton, P. Li, M. Malac, Radiation damage in the TEM and SEM, Micron 35 (2004) 399–409.
[11] R.M. Glaeser, Limitations to significant information in biological electron microscopy as a result of radiation damage, J. Ultrastruct. Res. 36 (1971) 466–482.
[12] J.M. Rowe, J.R. Dunlap, C.J. Gobler, et al., Isolation of a non-phage-like lytic virus infecting *Aureococcus anophagefferens*, J. Phycol. 44 (2008) 71–76.
[13] S. Thiberge, A. Nechushtan, D. Sprinzak, et al., Scanning electron microscopy of cells and tissues under fully hydrated conditions, Proc. Natl. Acad. Sci. U. S. A. 101 (2004) 3346–3351.
[14] N. de Jonge, D.B. Peckys, G.J. Kremers, et al., Electron microscopy of whole cells in liquid with nanometer resolution, Proc. Natl. Acad. Sci. U. S. A. 106 (2009) 2159–2164.
[15] I. Solomonov, D. Talmi-Frank, Y. Milstein, et al., Introduction of correlative light and airSEM™ microscopy imaging for tissue research under ambient conditions, Sci. Rep. 4 (2014) 5987.
[16] L. Muscariello, F. Rosso, G. Marino, et al., A critical overview of ESEM applications in the biological field, J. Cell. Physiol. 205 (2005) 328–334.
[17] T. Ogura, Direct observation of unstained biological specimens in water by the frequency transmission electric-field method using SEM, PLOS One 9 (2014) e92780.
[18] T. Ogura, Non-destructive observation of intact bacteria and viruses in water by the highly sensitive frequency transmission electric-field method based on SEM, Biochem. Biophys. Res. Commun. 450 (2014) 1684–1689.
[19] T.G. Lilburn, C.E. Haith, R.C. Prince, et al., Pleiotropic effects of *pufX* gene deletion on the structure and function of the photosynthetic apparatus of *Rhodobacter capsulatus*, Biochim. Biophys. Acta 1100 (1992) 160–170.
[20] F. Oling, E.J. Boekema, I.O. de Zarate, et al., Two-dimensional crystals of LH2 light-harvesting complexes from *Ectothiorhodospira sp.* and *Rhodobacter capsulatus* investigated by electron microscopy, Biochim. Biophys. Acta 1273 (1996) 44–50.
[21] K.J. Shelswell, T.A. Taylor, J.T. Beatty, Photoresponsive flagellum-independent motility of the purple phototrophic bacterium *Rhodobacter capsulatus*, J. Bacteriol. 187 (2005) 5040–5043.
[22] K. Yonekura, S. Maki-Yonekura, K. Namba, Complete atomic model of the bacterial flagellar filament by electron cryomicroscopy, Nature 424 (2003) 643–650.

[23] C.A. Fux, J.W. Costerton, P.S. Stewart, et al., Survival strategies of infectious biofilms, Trends Microbiol. 13 (2005) 34–40.
[24] J.A. Hobot, W. Villiger, J. Escaig, et al., Shape and fine-structure of nucleoids observed on sections of ultrarapidly frozen and cryosubstituted bacteria, J. Bacteriol. 162 (1985) 960–971.
[25] M. Eltsov, B. Zuber, Transmission electron microscopy of the bacterial nucleoid, J. Struct. Biol. 156 (2006) 246–254.
[26] P. Allan-Wojtas, L.T. Hansen, A.T. Paulson, Microstructural studies of probiotic bacteria-loaded alginate microcapsules using standard electron microscopy techniques and anhydrous fixation, LWT Food Sci. Technol. 41 (2008) 101–108.
[27] G.F. Rohrmann, Baculovirus structural proteins, J. Gen. Virol. 73 (1992) 749–761.
[28] G.H. Bergold, The molecular structure of some insect virus inclusion bodies, J. Ultrastruct. Res. 8 (1963) 360–378.
[29] N. van Loo, E. Fortunati, E. Ehlert, et al., Baculovirus infection of nondividing mammalian cells: mechanisms of entry and nuclear transport of capsids, J. Virol. 75 (2001) 961–970.
[30] A. Feinstei, E.A. Munn, Conformation of free and antigenbound IgM antibody molecules, Nature 224 (1969) 1307–1309.
[31] E.A. Munn, L. Bachmann, A. Feinstein, Structure of hydrated immunoglobulins and antigen-antibody complexes: electron microscopy of spray-freeze-etched specimens, Biochim. Biophys. Acta 625 (1980) 1–9.
[32] D.M. Czajkowsky, Z. Shao, The human IgM pentamer is a mushroom-shaped molecule with a flexural bias, Proc. Natl. Acad. Sci. U. S. A. 106 (2009) 14960–14965.
[33] T. Ogura, Three-dimensional X-ray observation of atmospheric biological samples by linear-array scanning-electron generation X-ray microscope system, PLOS One 6 (2011) e21516.